Escherichia coli Colonization of Intestinal Epithelial Layers In Vitro in the Presence of Encapsulated Bifidobacterium breve for Its Protection against Gastrointestinal Fluids and Antibiotics

Yuan, Lu; Wei, Hao; Yang, Xiao-Yu; Geng, Wei; Peterson, Brandon W.; van der Mei, Henny C.; Busscher, Henk J.

Published in:
ACS Applied Materials & Interfaces

DOI:
10.1021/acsami.0c21790

Publication date:
2021

ACS APPLIED MATERIALS & INTERFACES

www.acsami.org

Research Article

Escherichia coli Colonization of Intestinal Epithelial Layers *In Vitro* in the Presence of Encapsulated *Bifidobacterium breve* for Its Protection against Gastrointestinal Fluids and Antibiotics

Lu Yuan, Hao Wei, Xiao-Yu Yang, Wei Geng, Brandon W. Peterson, Henny C. van der Mei,* and Henk J. Busscher*

Cite This: *ACS Appl. Mater. Interfaces* 2021, 13, 15973−15982

Read Online

ACCESS | Metrics & More | Article Recommendations | Supporting Information

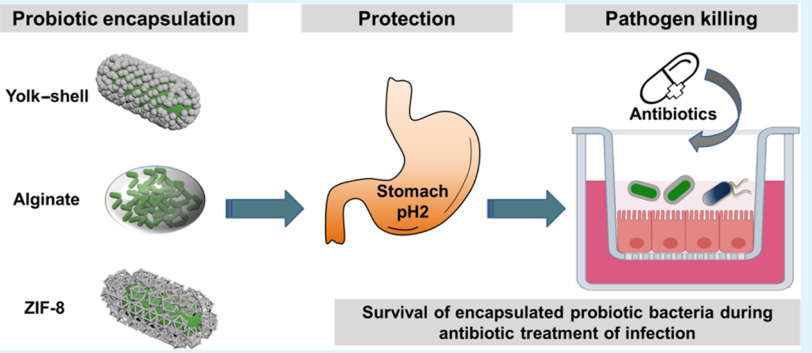

ABSTRACT: Encapsulation of probiotic bacteria can enhance their functionality when used in combination with antibiotics for treating intestinal tract infections. The interaction strength of encapsulating shells, however, varies among the encapsulation methods and impacts encapsulation. Here, we compared the protection offered by encapsulating shells with different interaction strengths toward probiotic *Bifidobacterium breve* against simulated gastric fluid and tetracycline, including protamine-assisted SiO_2 nanoparticle yolk−shell packing (weak interaction across a void), alginate gelation (intermediate interaction due to hydrogen binding), and ZIF-8 mineralization (strong interaction due to coordinate covalent binding). The presence of encapsulating shells was demonstrated using X-ray-photoelectron spectroscopy, particulate microelectrophoresis, and dynamic light scattering. Strong interaction upon ZIF-8 encapsulation caused demonstrable cell wall damage to *B. breve* and slightly reduced bacterial viability, delaying the growth of encapsulated bacteria. Cell wall damage and reduced viability did not occur upon encapsulation with weakly interacting yolk−shells. Only alginate-hydrogel-based shells yielded protection against simulated gastric acid and tetracycline. Accordingly, only alginate-hydrogel-encapsulated *B. breve* operated synergistically with tetracycline in killing tetracycline-resistant *Escherichia coli* adhering to intestinal epithelial layers and maintained surface coverage of transwell membranes by epithelial cell layers and their barrier integrity. This synergy between alginate-hydrogel-encapsulated *B. breve* and an antibiotic warrants further studies for treating antibiotic-resistant *E. coli* infections in the gastrointestinal tract.

KEYWORDS: *yolk−shell, alginate hydrogel, ZIF-8, intestinal infection, microbiomes, probiotics*

INTRODUCTION

Encapsulation of probiotic bacteria can enhance the functionality of probiotics in over-the-counter food and beverages and in the clinical control of bacterial infections. Probiotics provide health benefits, in particular, to the lower gastrointestinal tract, most notably by maintaining or restoring a balanced intestinal microflora.[1−4] However, this can only be achieved if, after oral administration, probiotic bacteria can reach their intestinal target site in a viable state.[5] This is not trivial, however, since during passage through the gastrointestinal tract, exposure to acidic conditions can severely hamper their viability.[6−8] Lactobacilli and Bifidobacteria are the most commonly applied probiotics associated with gastrointestinal health.[9,10] Whey protein spray-drying has been employed to encapsulate probiotic Bifidobacteria in fermented dairy products to facilitate their survival in simulated gastrointestinal conditions.[11,12] Alginate gelation has been shown to protect encapsulated Lactobacilli against acidic conditions,[13] as encountered by probiotic bacteria underway in the gastro-

Received: December 8, 2020
Accepted: March 23, 2021
Published: April 1, 2021

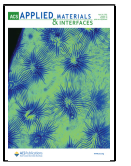

intestinal tract toward their intestinal target site. Beyond their use in over-the-counter products, a combination of probiotic Lactobacilli encapsulated in an alginate hydrogel and tobramycin has recently been demonstrated to synergistically kill a methicillin-resistant *Staphylococcus aureus* strain.[14] Clinically, synergistic use of antibiotics and probiotic bacteria without encapsulation in a protective shell will generally be impossible in the treatment of intestinal tract infections, as the antibiotics that are supposed to kill the infectious pathogens will also kill the probiotic bacteria.[15,16]

The yolk−shell is an example of a highly cell-friendly mineralized encapsulating shell.[17] An important characteristic of the yolk−shell responsible for its cell friendliness is the absence of binding between the shell and the bacterial cell surface. In yolk−shell encapsulation, the SiO_2 nanoparticles self-assemble on a pre-adsorbed protamine film on a bacterial cell surface. The protamine film internalizes into the bacterium after self-assembly of the nanoparticles to form a void between the bacterial cell surface and the nanoparticle shell,[17] across which only a weak interaction is resulted. Yolk−shell encapsulation has not yet been employed for probiotic bacteria. Alginate, electrostatically crosslinked by Ca^{2+} ions, has been frequently employed for encapsulating probiotic bacteria.[18] Alginate gelation is relatively simple and inexpensive, yielding an extensive three-dimensional hydrogel[13,19] that interacts with bacterial cell surface proteins through hydrogen binding with carboxyl and hydroxyl groups in the alginate hydrogel.[20] In a hydrogen bond, a shared electron pair is formed between a hydrogen atom and another atom, giving rise to weak interactions with typical binding energies up to 4 kcal mol^{-1}.[21] However, due to the high porosity of many hydrogels, encapsulated bacteria may remain sensitive to extreme pH conditions. Another new type of encapsulating shell not yet applied for probiotic protection is based on mineralization of a 2-methylimidazole zinc-salt based metal−organic framework (ZIF-8).[22] Zn has very low toxicity, and mineralized shells with ZIF-8 yield high viability and possess high porosity. The ZIF-8-mineralized shells interact with the amino groups of bacterial cell surface proteins through coordinate covalent binding with zinc.[23] In contrast to hydrogen binding, coordination covalent binding involves electrons from only one of the interacting atoms to form a shared electron pair with another atom, yielding strong interactions, for example, zinc with amino acid side chains between 195 and 364 kcal mol^{-1}, depending on the coordination geometry.[24]

This study aimed to compare the protection offered by encapsulating shells with different interaction strengths toward a probiotic *Bifidobacterium breve* against simulated gastric fluid (SGF) and tetracycline. To this end, *B. breve* was encapsulated using protamine-assisted SiO_2 nanoparticle packing, alginate gelation, and ZIF-8 mineralization. The physicochemical properties of unencapsulated and differently encapsulated Bifidobacteria, as well as the protection offered toward SGF and tetracycline, were determined. As a proof of the pudding, killing of pathogenic *Escherichia coli* biofilms grown on an intestinal epithelial layer in a transwell by differently encapsulated Bifidobacteria in the absence and presence of tetracycline was evaluated after their exposure to SGF. In addition, pathogen-inflicted damage to the integrity of the cellular layer was assessed microscopically and using trans-epithelial electrical resistance (TEER)[25] measurements across the intestinal epithelial layer.

EXPERIMENTAL SECTION

Materials and Reagents. *B. breve* ATCC15700 and Caco-2 BBe1 (ATCC CRL-2102) intestinal epithelial cells were purchased from American Type Culture Collection (ATCC, Manassas, VA, USA). Lysogeny broth (LB), tetracycline hydrochloride, protamine, 2-methylimidazole, LUDOX HS-40 colloidal silica, zinc acetate dihydrate, pepsin, phalloidin-FITC, and 4′,6-diamidino-2-phenylindole dihydrochloride (DAPI) were obtained from Sigma-Aldrich (St. Louis, MO, USA); reinforced clostridial medium (RCM) was obtained from Becton & Dickinson (Franklin Lakes, NJ, USA), and Dulbecco's modified Eagle medium containing 4.5 g/L glucose (DMEM-HG), fetal bovine serum (FBS), and trypsin−EDTA (2.5 g/L) were obtained from Gibco (Gaithersburg, MD, USA). Transwells (12 well-plates) with 0.4 μm poly(ethylene terephthalate) (PET) porous membranes were purchased from Greiner Bio-One (Österreich, Austria). The Live/Dead BacLight Bacterial Viability Kit was obtained from Thermo Fisher Scientific (Waltham, Massachusetts, USA).

Bacterial Culturing and Harvesting. *B. breve* ATCC15700 was streaked on RCM agar plates from a frozen stock and grown under anaerobic conditions (85% N_2, 5% CO_2, and 10% H_2) at 37 °C for 48 h. *E. coli* Hu734 is a tetracycline-resistant (see Figure S1) human clinical isolate and used as a pathogenic strain. *E. coli* was streaked on a blood agar plate and aerobically incubated at 37 °C for 24 h. Subsequently, one *B. breve* colony was transferred to the RCM broth and an *E. coli* colony was transferred to the LB broth. Strains were cultured for 24 h after which the bacteria were transferred (1:20) to their respective fresh culture media and grown for 18 h under appropriate conditions. The bacteria were harvested by centrifugation for 5 min at 6500*g* at 10 °C, washed twice with sterile 10 mM potassium phosphate buffer (5 mM K_2HPO_4, 5 mM KH_2PO_4, pH 7.0), and re-suspended in 10 mM phosphate buffer for further use. The concentrations of *B. breve* and *E. coli* were determined by enumeration in a Bürker-Türk counting chamber and adjusted to a concentration appropriate for the respective experiments.

Encapsulation Methods Applied. An alginate-hydrogel-based method and a two-nanobiomaterial-based method were used to encapsulate *B. breve*. For protamine-assisted SiO_2 nanoparticle encapsulation of *B. breve* (*B. breve*@SiO_2), *B. breve* (3×10^8/mL) suspended in a 1 mg/mL protamine solution in 10 mM phosphate buffer by vortexing for 1 min[17] were allowed to settle for 15 min at room temperature. Bacteria were collected by centrifugation at 6500*g* at 10 °C for 5 min and re-suspended in 1 mg/mL SiO_2 nanoparticle (12 nm diameter according to the LUDOX HS-40 product specification) suspension in 10 mM potassium phosphate buffer. The mixture was vortexed for 1 min, and the encapsulated bacteria were allowed to settle at room temperature for another 15 min. Finally, *B. breve*@SiO_2 were collected by centrifugation (6500*g* at 10 °C for 5 min) and re-suspended in 10 mM phosphate buffer for further use.

Alginate hydrogel encapsulation of *B. breve* (*B. breve*@Alginate) was done as previously described with minor modifications.[14] Briefly, *B. breve* (3×10^9/mL), suspended in 5 mL of 10 mM phosphate buffer with 25 mg/mL of alginate, was vortexed for 1 min. Subsequently, the mixture of *B. breve* with alginate was dropwise added into 50 mL of 0.1 M $CaCl_2$ solution and stirred for 30 min at room temperature to allow complete gelation. In order to obtain protective shells with different thicknesses, the droplet volumes were varied from 5 μL up to 20 μL. Finally, *B. breve*@Alginate were collected by filtration and stored in 10 mM phosphate buffer.

ZIF-8 encapsulation of *B. breve* (*B. breve*@ZIF-8) was done by suspending *B. breve* (3×10^9/mL) in 5 mL of demineralized water containing 160 mM 2-methylimidazole.[22] Subsequently, 5 mL of 40 mM zinc acetate dihydrate in demineralized water was added, and the mixture was kept at 37 °C under shaking for 10 min (150 rpm). After shaking, the encapsulated *B. breve* were collected by centrifugation at 6500*g* at 10 °C for 5 min and re-suspended in 10 mM phosphate buffer.

https://doi.org/10.1021/acsami.0c21790
ACS Appl. Mater. Interfaces 2021, 13, 15973−15982

Elemental Surface Composition, Zeta Potentials, and Diameters of Encapsulated Bacteria. The elemental surface compositions, zeta potentials, and diameters of unencapsulated and encapsulated *B. breve* were measured in order to demonstrate the presence of encapsulating shells. The elemental surface compositions of unencapsulated and encapsulated *B. breve* were determined using X-ray photoelectron spectroscopy (XPS; S-Probe, Surface Science Instruments, Mountain View, CA, USA). To this end, unencapsulated and encapsulated bacteria were washed twice with demineralized water and freeze-dried (Leybold, Germany). The freeze-dried bacterial powders were pressed into small stainless steel cups and put into the XPS chamber. The XPS chamber was equipped with an aluminum anode (10 kV, 22 mA), and overall scans were taken over the binding energy range of 1−1200 eV at a resolution of 150 eV and a spot size of 1000 × 250 μm. Narrow scans were taken over the binding energy range of 20 eV to determine the chemical functionalities in O_{1s}. The binding energies were calculated with respect to the C_{1s} binding energy peak set at 284.8 eV. The area under each peak, after background subtraction, was used for the calculation of peak intensities, yielding elemental surface concentration ratios for nitrogen, oxygen, and phosphorus to carbon.

The zeta potentials (through particulate microelectrophoresis) and diameters (through dynamic light scattering) of unencapsulated and encapsulated *B. breve* were measured on a Malvern ZetaSizer ZEN3600 instrument (Malvern Panalytical, Worcestershire, UK) in 10 mM potassium phosphate buffer (bacterial concentration 3×10^7/mL) over the pH range of 2−9; the pH was adjusted by 0.1 M HCl or 0.1 M KOH. The diameters were only measured at pH 7.0.

Viability of *B. breve* after Encapsulation. In order to assess adverse effects of encapsulation on the viability of *B. breve*, the number of viable *B. breve* before and after encapsulation were determined by colony-forming units (CFUs). Prior to assessing the viability, yolk−shells were removed by sonication for 30 s at 130 W while cooling in an ice−water bath, alginate-hydrogel-based shells were removed by a 15 min exposure to a 55 mM sodium citrate solution, and ZIF-8-mineralized shells were removed by exposure to 10 mM EDTA for 5 min. After the removal of the shells, the bacteria were collected by centrifugation (6500*g* at 10 °C for 5 min) and re-suspended in 10 mM potassium phosphate buffer. Serial dilutions of the resulting bacterial suspensions were made in phosphate buffer and plated on RCM agar. After anaerobic culturing of the RCM agar plates, the numbers of CFU were enumerated.

In addition, possible growth inhibition of *B. breve* by different encapsulating shells was determined without shell removal in modified growth medium (70% DMEM-HG supplemented with 30% RCM) that allows the growth of *B. breve*, *E. coli*, and intestinal epithelial cells.[26] Bacterial growth was monitored for 24 h and quantitated by measuring OD_{600} (Genesy30, Thermo Scientific). The modified medium without bacteria was used as a blank control.

Cell wall integrity before and after encapsulation was assessed using SYTO9/propidium iodide staining (BacLight Bacterial Viability Kit), rendering bacteria without cell wall damage green fluorescence and bacteria with cell wall damage red fluorescence, respectively. Briefly, unencapsulated *B. breve* and bacteria after shell removal (3×10^8/mL) were stained with SYTO9/propidium iodide solution and incubated in the dark at room temperature for 15 min, after which bacterial fluorescence was examined using fluorescence microscopy (Leica DM4000, Germany).

Protection of *B. breve* Encapsulation against SGF and Tetracycline. The protection offered by the different encapsulations of *B. breve* was evaluated against SGF (SGF) and the antibiotic tetracycline. SGF was prepared by dissolving 2.0 g of NaCl and 6.0 g of pepsin in 7 mL of 37% HCl.[27] Next, the solution was diluted with demineralized water to 1 L and pH was adjusted to pH 2 by adding 1 M NaOH. SGF was filtered (0.22 μm filter) prior to use. In order to evaluate the protection offered by the different encapsulations, unencapsulated and differently encapsulated *B. breve* were suspended at a concentration of 3×10^8/mL in SGF under shaking of 150 rpm at 37 °C. Depending on the amount, composition, and size of a meal, the complete passage of food through the stomach requires 2−4 h. However, within 20 min after consuming solid food, the first food leaves the stomach, while 50% of water after consuming a single glass of water would have passed through the stomach after 10 min.[28] Hence, we chose 30 min as the exposure time for evaluating the protection offered by encapsulating shells against SGF. After 30 min of exposure to SGF, bacteria were collected by centrifugation (6500*g* for 5 min), washed with 10 mM phosphate buffer, and re-suspended in 10 mM phosphate buffer. Only *B. breve*@Alginate was collected by filtration. The bacterial suspensions with unencapsulated and differently encapsulated bacteria were serially diluted and plated on RCM agar. After 48 h of growth under anaerobic conditions, the numbers of CFUs were enumerated.

Protection of different encapsulations against tetracycline was evaluated by culturing unencapsulated and encapsulated *B. breve* (3×10^8/mL) in a modified medium supplemented with tetracycline (10 μg/mL) for 3 h. After culturing, *B. breve* were collected by centrifugation, washed with phosphate buffer, serially diluted, and plated on RCM agar for CFU enumeration, as described above.

***B. breve* Protection of Intestinal Epithelial Cells against an *E. coli* Challenge in the Absence or Presence of Tetracycline.** Human intestinal epithelial cells (Caco-2 BBe) were grown in DMEM-HG supplemented with 10% (vol/vol) FBS in 5% CO_2 humidified air at 37 °C. Cells were passaged at 80% confluency after trypsinization using trypsin−EDTA at 37 °C for 5 min. After detachment, 6 mL of DMEM-HG with 10% FBS was added for trypsin neutralization and cells were collected by centrifugation at 800*g* for 5 min. The cellular pellet was re-suspended in DMEM-HG supplemented with 10% FBS, and their concentration was adjusted to 2×10^5 cells/mL by counting in a Bürker-Türk counting chamber. Then, 0.5 mL of cell suspension was added to a transwell insert in a 12-well plate with a 1.13 cm^2 PET membrane (pore size 0.4 μm). During the growth of the cellular layer, the medium was refreshed every other day. The integrity of the cellular layer was monitored by measuring its TEER using a MillicellERS-2 meter (Millipore, USA). Within 10−14 days, the TEER had reached a value ≥400 Ω × cm2, characteristic of an intestinal epithelial monolayer, and the layer was used for further experiments.

First, unencapsulated and differently encapsulated *B. breve* after having been exposed to SGF as described above were added on the intestinal epithelial layer in the transwell at a final concentration of 3×10^8/mL, and further co-culturing of *B. breve* and epithelial cells was continued in modified growth medium (70% cell culture medium supplemented with 30% RCM).[26] After 4 h of co-culturing epithelial cells with adhering *B. breve*, the cell layer with *B. breve* was challenged with an *E. coli* suspension (50 μL, concentration 3×10^7/mL) in 10 mM phosphate buffer, and co-culturing was continued in a 5% CO_2 humidified incubator at 37 °C for another 24 h.

To evaluate the combined effects of probiotic *B. breve* and tetracycline on the eradication of an infectious *E. coli* biofilm, unencapsulated and encapsulated *B. breve* exposed to SGF as described above were added to the intestinal epithelial cell layer on the transwell membrane at a concentration of 3×10^8/mL. After co-culturing with the modified medium for 4 h, the cell layer was challenged with an *E. coli* suspension (50 μL, concentration 3×10^7/mL) in 10 mM phosphate buffer. Two hours after initiating the *E. coli* challenge, tetracycline was added for 3 h at a final concentration of 10 μg/mL. After 3 h, the modified medium was refreshed and culturing continued in the absence of tetracycline for another 19 h.

The TEER values of the intestinal epithelial layers were measured to monitor the intestinal barrier integrity before initiating the *E. coli* challenge and after 24 h, that is, the end point of an experiment. At the end of an experiment, the numbers of adhering *E. coli* and *B. breve* were determined. To this end, the cell layers with adhering bacteria were washed twice with phosphate-buffered saline (PBS), and 200 μL of trypsin−EDTA (2.5 mg/mL) was added for 5 min at 37 °C to detach the cell layers from the transwell membrane. The bacterial cell suspension was subsequently mixed with 300 μL of PBS and vortexed for 30 s. The resulting bacterial cell suspension was centrifuged (6500*g* for 5 min) to remove the trypsin and re-suspended in 0.5 mL of PBS. After serial dilution, the suspension was plated on LB agar

https://doi.org/10.1021/acsami.0c21790
ACS Appl. Mater. Interfaces 2021, 13, 15973−15982

plates to grow *E. coli* and on RCM agar to grow *B. breve* (for details, see section "Bacterial Culturing and Harvesting"). After 24 h of growth the number of CFUs of *E. coli* was counted and after 48 h the number of CFUs of *B. breve* was counted to yield the numbers of *B. breve* and *E. coli* adhering to the epithelial cell layers. The intestinal epithelial cells on the transwell membranes were stained with phalloidin-FITC (F-actin) and DAPI (DNA). Briefly, the cells were washed with PBS buffer for 5 min, fixed with 3.7% (wt/vol) paraformaldehyde for 15 min, and permeabilized with 0.5% (vol/vol) Triton X-100 for another 5 min. Subsequently, the cells were stained with phalloidin-FITC (diluted 50× in PBS with 1% bovine serum albumin) and DAPI (diluted 50× in PBS with 1% bovine serum albumin) for 30 min and then washed with PBS. The cells were imaged using fluorescence microscopy (Leica DM4000, Germany), and surface coverage was determined using Fiji software.[29] Five images per sample were averaged.

Statistical Analysis. All experiments were carried out in triplicate with separately cultured cells and bacteria. Results were expressed as means ± standard deviation (SD) and analyzed with one-way analysis of variance (ANOVA), followed by Dunnett's or Tukey's test for multiple comparison using GraphPad Prism 8.00. Differences between groups at $p < 0.05$ were considered as statistically significant.

RESULTS

Characterization of Unencapsulated and Differently Encapsulated *B. breve*. XPS presents an easy way to obtain elemental surface compositions of bacterial cell surfaces[30,31] and therewith demonstrate successful encapsulation. Unencapsulated *B. breve* demonstrated C_{1s}, O_{1s}, and N_{1s} electron binding energies (Figure 1A) of which nitrogen is uniquely associated with surface proteins.[32,33] Confirmation of the association of nitrogen with surface proteins was obtained from a decomposition of the O_{1s} binding energy spectrum (Figure S2A), showing a binding energy component at 531.5 eV due to C═O and N−C═O functionalities. Yolk−shell encapsulation through SiO_2 nanoparticle assembly reduced elemental surface concentrations of carbon, nitrogen, and phosphorus (Table 1), while oxygen and silicon appeared in a ratio of 2.1. This ratio confirms full encapsulation of bacteria with SiO_2 nanoparticles with a thickness that, in a freeze-dried state, exceeds the XPS depth of information, that is, around 5 nm.[34] The presence of SiO_2 nanoparticles was furthermore confirmed by decomposition of the O_{1s} electron binding energy spectrum (Figure S2B), demonstrating Si−O as the major component in the shell. Alginate hydrogel encapsulation also reduced nitrogen counts (Table 1), but O_{1s} peak components representative of cell surface proteins remained detectable (Figure S2C), probably because the hydrogel shell collapsed into a thin layer upon freeze-drying as required for XPS analysis. Alginate gelation uniquely introduced calcium involved in bridging of the anionic polymer chains within the hydrogel network.[35] ZIF-8-mineralized shells were evidenced by the presence of zinc, together with high amounts of nitrogen from 2-methylimidazole ligands, used for coordinate covalent binding between zinc and the amino groups of bacterial surface proteins. Narrow scans of the O_{1s} electron binding energies also demonstrated components representative of C═O and N−C═O functionalities underlying the shell (Figure S2D), indicative of a relatively thin shell with a dehydrated thickness within the XPS depth of information.

The zeta potentials of unencapsulated *B. breve* were negative over the entire pH range from pH 2 to 9 (Figure 1B). Protamine-assisted, SiO_2 nanoparticle yolk−shells caused less negative zeta potentials over the entire pH range with a well-defined iso-electric point at pH 3.4, coinciding with the iso-

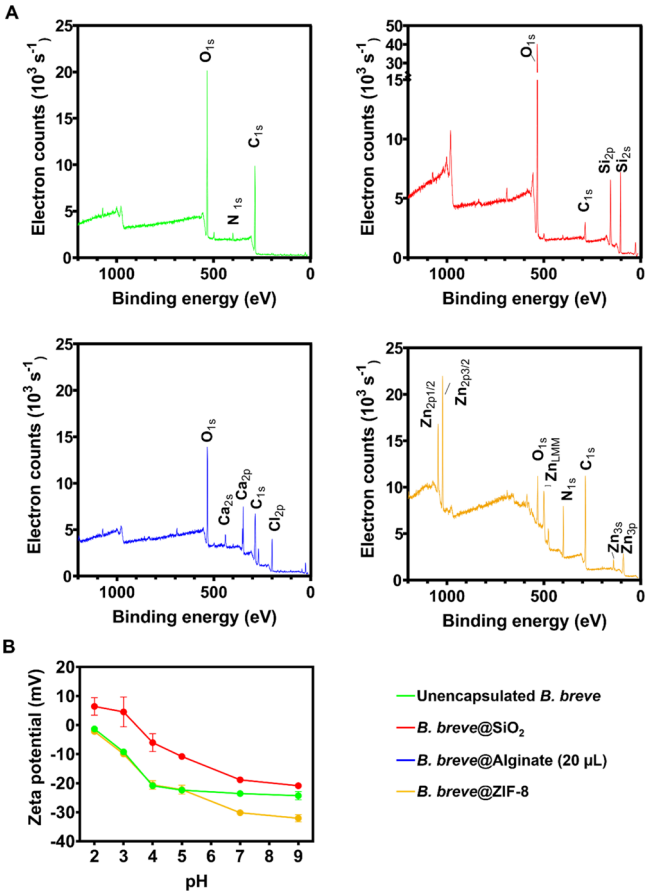

Figure 1. Characterization of unencapsulated and differently encapsulated *B. breve* ATCC15700 using XPS and particulate microelectrophoresis. (A) Wide scan electron binding energy spectra of unencapsulated and differently encapsulated *B. breve*. (B) Zeta potentials of unencapsulated and differently encapsulated *B. breve* measured in phosphate buffer (5 mM K_2HPO_4 and 5 mM KH_2PO_4) as a function of pH. Note that alginate-encapsulated *B. breve* in their fully hydrated state were too large for particulate microelectrophoresis. Error bars represent the SD over three experiments with separately grown bacteria. Note that for *B. breve*@Alginate, 20 μL alginate droplets were used for encapsulation.

electric point of SiO_2 nanoparticles.[36] Internalization of pre-adsorbed protamine was confirmed by time-dependent zeta potential measurements and Fourier transform infrared spectroscopy (FTIR) of *B. breve* after protamine adsorption (Figure S3). Protamine adsorption caused an initial increase of *B. breve* zeta potentials to positive values between pH 3 and 6 (Figure S3A), while FTIR spectra (Figure S3B−D) demonstrated a strong increase in AmI (1653 cm^{-1}) and AmII (1541 cm^{-1}) absorption band ratios with respect to the C−H (around 2930 cm^{-1}) absorption band (Figure S3). However, 1 h after protamine adsorption, the zeta potentials returned to the same values as observed before protamine adsorption but amide absorption band ratios remained invariably high (Figure S3E). Since the zeta potentials reflect only the outer cell surface, while the FTIR spectra represent the composition of both the cell interior and its surface, which indicated the internalization of the adsorbed protamine. ZIF-8 encapsulation only affected *B. breve* zeta potentials in the pH range of 7−9 (see also Figure 1B). This may implicate that the ZIF-8 shell acts as a soft layer[37] below pH 7, positioning the plane of shear inside the shell close to the bacterial cell surface and measuring

https://doi.org/10.1021/acsami.0c21790
ACS Appl. Mater. Interfaces 2021, 13, 15973−15982

Table 1. Elemental Surface Composition of Freeze-Dried, Unencapsulated and Differently Encapsulated *B. breve* ATCC15700[a]

encapsulation method	C (%)	O (%)	N (%)	P (%)	Ca (%)	Si (%)	Zn (%)
unencapsulated	64.4	32.1	2.1	0.2			
yolk−shell, SiO_2 nanoparticle assembly	9.8	59.5	0.6			28.8	
alginate gelation[b]	51.7	28.7	0.7	0.5	7.4	1.3	
ZIF-8 mineralization	61.1	13.3	16.9				8.3

[a]Na, Cl, and F were not included in this table. [b]20 μL alginate droplets were used for encapsulation.

the zeta potentials identical to those of unencapsulated bacteria. Positioning the plane of shear within the shell while still probing the bacterial cell surface charge confirms that the ZIF-8 shell is relatively thin. Above pH 7, however, deprotonation of imidazole groups may interfere with electrophoretic probing of charges closely connected with the cell surface to yield more negative zeta potentials. The zeta potentials of hydrated alginate-hydrogel-encapsulated *B. breve* could not be determined because bacteria with a hydrated alginate shell were too large for particulate microelectrophoresis using the Malvern ZetaSizer ZEN3600.

Unencapsulated *B. breve* in their hydrated state had a diameter of 998 ± 17 nm with a low polydispersity index (0.18). Diameters increased to 1190 ± 177 and 1141 ± 184 nm upon yolk−shell and ZIF-8 encapsulation, respectively, while polydispersity indices increased to 0.39 and 0.69, respectively. These diameters and polydispersities are all within the micrometer-range size of bacteria, indicating single-cell encapsulation. The diameter of hydrated, alginate-hydrogel-encapsulated *B. breve* was too large for measurement using dynamic light scattering due to the size of the hydrated alginate gel, possibly comprising more than one bacterium.

Cell Wall Damage, Viability, and Growth Curves of *B. breve* after Encapsulation. Different encapsulations inflicted different types of damages to *B. breve* (Figure 2). Neither alginate gelation nor protamine-assisted, SiO_2 nanoparticle assembly caused any cell wall damage (Figure 2A). ZIF-8 mineralization, however, yielded clear cell wall damage probably as a result of its strong coordinate covalent binding between bacterial cell surface proteins and zinc.

After the removal of encapsulating shells, *B. breve* could be grown on agar plates in the same numbers of CFUs as *B. breve* that had never been encapsulated. From this, it can be concluded that neither encapsulation nor shell removal had a negative impact on bacterial viability. Only the cell wall damage inflicted by ZIF-8 mineralization was accompanied by a small decrease in bacterial viability after encapsulation (Figure 2B). Neither type of encapsulation inhibited bacterial growth, and all growth curves demonstrated standard kinetics, including a lag phase and an exponential growth phase leading to a stationary phase. However, all the three different types of encapsulations delayed bacterial growth as compared with unencapsulated *B. breve* (Figure 2C), indicative of recovery from encapsulation and growth through the shell. The onset of the exponential growth phase was delayed least by weakly interacting, protamine-assisted, SiO_2 nanoparticle yolk−shell packing, probably due to the absence of direct contact between the shell and the bacterial cell surface. In line with the cell wall damage and minor reduction in viability of *B. breve* upon ZIF-8 mineralization of a shell, recovery from encapsulation and growth through the shell lasted longest and the onset of exponential growth was delayed most by ZIF-8 shells.

Protection Offered to Planktonic *B. breve* by Different Shells against Low pH and Antibiotic Exposure in the Absence of *E. coli*. Unencapsulated *B. breve* did not survive exposure to SGF at pH 2 (Figure 3A) and only alginate hydrogel gelation prepared with 20 μL droplets provided a shell that was able to effectively protect *B. breve* against 30 min of exposure to simulated gastric acid. Alginate hydrogel shells prepared with droplet volumes smaller than 20 μL did not offer effective protection against simulated gastric acid (Figure S4). Hence, all data in the remainder of this paper, including the conclusions, pertain on alginate hydrogel encapsulation prepared using 20 μL droplets. Exposure of *B. breve* (3×10^8/mL) to tetracycline (10 μg/mL) yielded a 2 log unit reduction in CFUs compared with a PBS control. Shells prepared by alginate gelation caused full protection against tetracycline. None of the other shells could achieve this level of protection, and encapsulating shells composed of nanobiomaterials caused even greater reductions in CFUs upon tetracycline exposure than experienced by unencapsulated *B. breve*. Thus, depending on the type of the protective shell

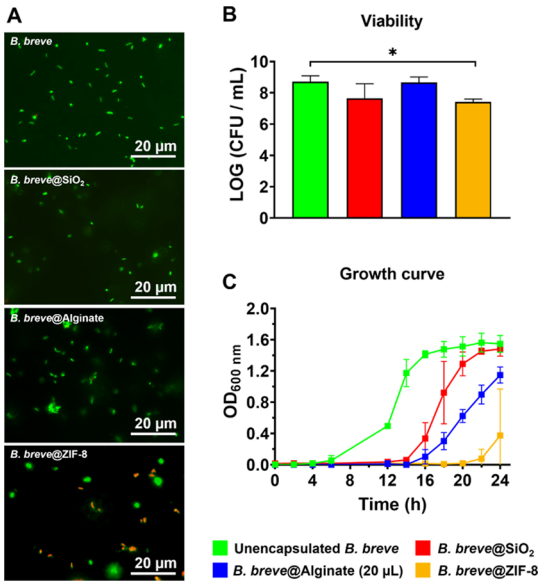

Figure 2. Cell wall damage, viabilities, and growth curves of differently encapsulated *B. breve* ATCC15700. (A) Cell wall damage (red fluorescent bacteria) inflicted to *B. breve* upon encapsulation. Shells have been removed before fluorescence staining and images have been enhanced for improved clarity. (B) Viability of *B. breve*, measured immediately after encapsulation, expressed as CFUs. Shells have been removed before agar plating. (C) Growth curve of unencapsulated and differently encapsulated *B. breve* expressed as OD_{600nm} as a function of time. Note that encapsulating shells have not been removed before starting a culture. Error bars represent the standard error of the mean (SEM) over three experiments with separately grown bacteria. * indicates statistically significant differences (one-way ANOVA, followed by Dunnett's test for multicomparison) between unencapsulated and encapsulated *B. breve*. Significance was accepted at $p < 0.05$. Note that for *B. breve*@Alginate, 20 μL alginate droplets were used for encapsulation.

https://doi.org/10.1021/acsami.0c21790
ACS Appl. Mater. Interfaces 2021, 13, 15973−15982

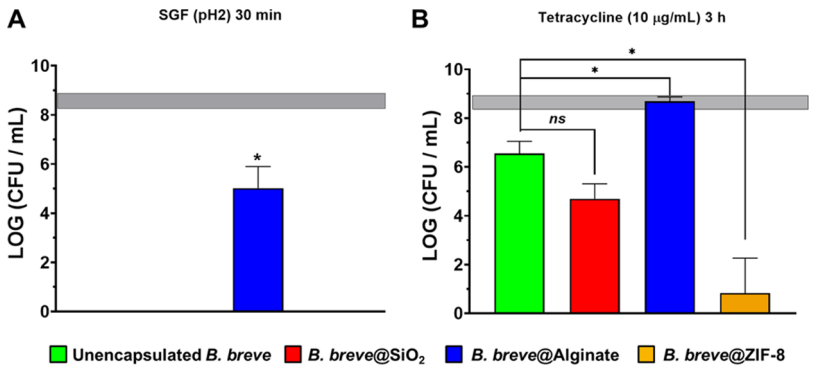

Figure 3. Protection by different shells offered to planktonic *B. breve* ATCC15700 in suspension against exposure to SGF (pH 2) or tetracycline. The horizontal bands represent CFU/mL ± SD after exposure of unencapsulated *B. breve* to PBS. (A) Survival of *B. breve* in suspension after 30 min of exposure to SGF (pH 2) for 30 min, expressed as CFUs. Shells have been removed before agar plating. The absence of data represents less than 10^2 CFU/mL. (B) Survival of *B. breve* in suspension after 3 h of exposure to tetracycline (10 μg/mL), expressed as CFUs. Shells have been removed before agar plating. Error bars represent the SEM over three experiments with separately grown bacteria. * indicates statistically significant differences (one-way ANOVA, followed by Tukey's test for multi-comparison) between unencapsulated and encapsulated *B. breve*. Significance was accepted at $p < 0.05$. The absence of significance is indicated as "ns".

applied, encapsulation may also backfire on the bacteria that were supposed to be protected by encapsulating shells.

Influence of Shell Components on the Viability of Planktonic *E. coli*. To evaluate whether shell components affected the viability of *E. coli*, alginate, SiO_2 nanoparticles, or ZIF-8 were cultured with *E. coli* in a modified growth medium. Neither alginate nor SiO_2 nanoparticles affected the viability of *E. coli*, while ZIF-8 slightly reduced the viability of *E. coli* (Figure S5).

Protection Offered by Differently Encapsulated *B. breve* to Intestinal Epithelial Cells against an *E. coli* Challenge. Finally, we evaluated the protection offered by differently encapsulated *B. breve* to a layer of intestinal epithelial cells against an *E. coli* challenge. Protection was evaluated with unencapsulated and encapsulated *B. breve* after 30 min of exposure to simulated gastric acid in order to mimic their oral administration. *B. breve* adhering to intestinal epithelial layers did not survive a challenge by pathogenic *E. coli*, except when encapsulated by an alginate hydrogel shell (Figure 4A) and regardless of tetracycline exposure (Figure 4B). *E. coli* adhering to intestinal epithelial layers were neither killed by unencapsulated nor killed by encapsulated *B. breve* (Figure 4C) or tetracycline alone (Figure 4D). However, the combined presence of surviving, alginate-hydrogel-encapsulated *B. breve* and tetracycline caused a significant, synergistic killing of adhering *E. coli* (see also Figure 4D) that other encapsulation methods did not achieve.

As a consequence, the *E. coli* challenges in the absence of tetracycline strongly impaired the barrier function of the epithelial layer regardless of the presence of (encapsulated) *B. breve*, as evidenced by a significant decrease in TEER to below the level of an unchallenged epithelial layer (Figure 4E). Concurrently, membrane surface coverage by epithelial cells derived from fluorescence imaging was absent (Figure 4G). However, fully in line with the synergistic killing of *E. coli* by alginate-encapsulated *B. breve* and tetracycline, the TEER values (Figure 4F) and membrane surface coverage by epithelial cells (Figure 4H) remained at the unchallenged level in the presence of alginate-encapsulated *B. breve* and tetracycline exposure. Other encapsulation methods did not achieve this synergistic protection of the intestinal epithelial layer.

DISCUSSION

Alginate-hydrogel-based shells yielded superior protection against simulated gastric acid and tetracycline as compared with nanobiomaterial-based shells, such as yolk–shell packing of SiO_2 nanoparticles or ZIF-8 mineralization. Accordingly, only alginate-hydrogel-encapsulated *B. breve* operated synergistically with tetracycline in killing tetracycline-resistant *E. coli* adhering to intestinal epithelial layers and maintaining surface coverage (Figure 4H) and barrier integrity (Figure 4F) of the cell layers.

The inability of nanobiomaterial-based shells to kill *E. coli* adhering to intestinal epithelial cell layers under antibiotic exposure is due to a combination of inadequate protective properties and cell wall damage caused during encapsulation. For yolk–shell encapsulation, the primary reason will be inadequate protection as it interacts weakly through a void[17] with encapsulated bacteria and no cell wall damage (Figure 2A) or reduction in viability (Figure 2B) was observed. Yolk–shell protection of *B. breve* offered no protection against simulated gastric acid (Figure 3A), and packed SiO_2 nanoparticle shells were unable to prevent penetration of acids. Possibly, bilayered shells, such as those composed of chitosan and alginate, are required to protect bacteria against SGF at pH 2, as observed for Bacillus coagulans, surviving around 3-logs more when encapsulated with chitosan and alginate applied through a layer-by-layer method rather than when encapsulated with a single layer composed of chitosan.[38] The yolk–shell, possessing pore diameters of around 11 nm, based on the use of 12 nm nanoparticles,[17] does protect against tetracycline. At this point, it is important to realize that protection of encapsulating shells against acidic conditions, antibiotics, and other potentially harmful substances is often temporary. Different shells may cause different delay times in the penetration of harmful substances, which suggests that adsorptive and absorptive properties of the shells may be more important than pore size. This is also true for the protection offered by alginate hydrogels toward *B. breve*, leaving the great majority of encapsulated *B. breve* viable after 30 min of exposure to SGF (see Figure 3A). However, a separate experiment demonstrated that protection decreased by 2-log units after 1 h as compared with 30 min of exposure to SGF, attesting to the temporary protection of bacterial

https://doi.org/10.1021/acsami.0c21790
ACS Appl. Mater. Interfaces 2021, 13, 15973−15982

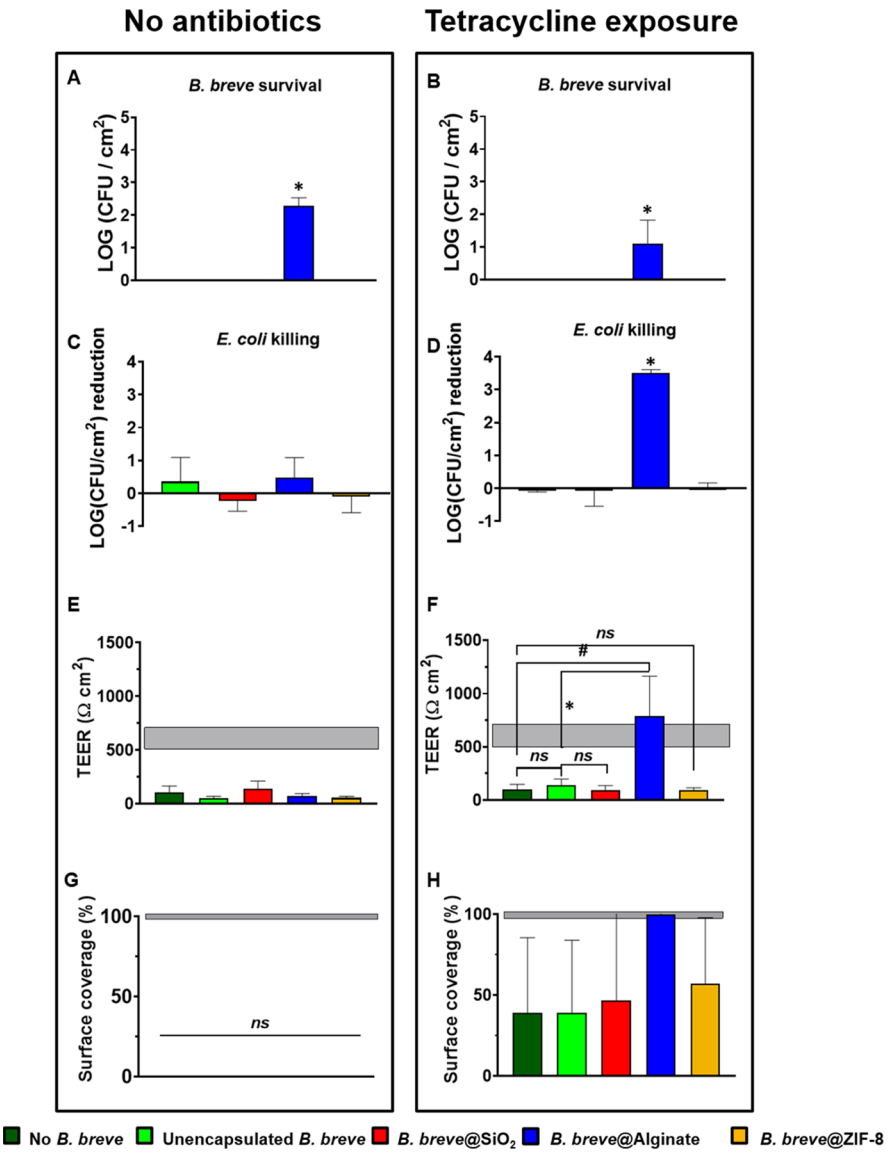

Figure 4. Effects of differently encapsulated *B. breve* ATCC15700 on their protection offered to intestinal epithelial layers against a 2 h *E. coli* Hu734 challenge in the absence or presence of tetracycline. Cell layers were co-cultured for 4 h with *B. breve* that were first exposed for 30 min to SGF, followed by a 2 h *E. coli* challenge and continued co-culturing for another 2 h. Finally, growth was pursued in the modified medium without or with tetracycline for another 22 h with tetracycline exposure for the first 3 h (10 μg/mL). (A) Number of *B. breve* CFUs adhering to intestinal epithelial layers that survived an *E. coli* challenge in the absence of tetracycline exposure. Absence of data indicates CFU/cm^2 below detection. (B) Same as panel (A), now for *B. breve* surviving an *E. coli* challenge in the presence of tetracycline exposure. Absence of data indicates CFU/cm^2 below detection. (C) The number of *E. coli* CFUs adhering to intestinal epithelial layers that were killed by differently encapsulated *B. breve* in the absence of tetracycline exposure. (D) Same as panel (C), now for *E. coli* killed by adhering differently encapsulated *B. breve* in the presence of tetracycline exposure. (E) TEER values of intestinal epithelial cell layers with adhering *B. breve* and challenged by *E. coli* in the absence of tetracycline exposure. The horizontal band represents the TEER values of intestinal cell layers with or without adhering *B. breve* in the absence of an *E. coli* challenge. Note that these TEER values were not affected by the presence of adhering unencapsulated or differently encapsulated *B. breve* (Figure S6A). (F) Same as panel (E), now for the TEER of intestinal epithelial cell layers with adhering *B. breve* and challenged by *E. coli* in the presence of tetracycline exposure. (G) Surface coverage of the transwell membrane by intestinal epithelial cell layers with adhering *B. breve* and challenged by *E. coli* in the absence of tetracycline exposure. The horizontal band represents the surface coverages of intestinal cell layers with or without adhering *B. breve* in the absence of an *E. coli* challenge (Figure S6B). Surface coverages were calculated from fluorescence images, as presented in Figure S6C. (H) Same as panel (G), but now representing surface coverage by intestinal epithelial cells of the transwell membrane in the presence of tetracycline exposure. The horizontal band represents the membrane surface coverage by intestinal cell layers without adhering *B. breve* in the absence of an *E. coli* challenge. Surface coverages were calculated from fluorescence images, as presented in Figure S6D. Error bars represent the SEM over three experiments with separately grown cells and bacteria. * indicates statistically significant differences (one-way ANOVA) between unencapsulated and encapsulated *B. breve*, while # indicates the difference between cellular layers with *E. coli* challenges in the absence of colonizing *B. breve* and in the presence of unencapsulated and encapsulated *B. breve*. Significance was accepted at $p < 0.05$. The absence of significance is indicated as "ns", while seemingly missing data are too close to the axes to be visible.

encapsulation. The combination of exposure to simulated gastric acid and tetracycline, mimicking the conditions encountered by an encapsulated probiotic bacterium on its way to an intestinal infection site while the patient is under

https://doi.org/10.1021/acsami.0c21790
ACS Appl. Mater. Interfaces 2021, 13, 15973−15982

antibiotic treatment, is too harsh, a condition for the yolk−shell to yield synergistic killing of *E. coli* adhering to an intestinal epithelial layer (Figure 4). For ZIF-8-mineralized shells, inadequate protection (Figure 3) is attributed to cell wall damage due to strong coordinate covalent binding of ZIF-8. Incidentally, cell wall damage upon ZIF-8 encapsulation has also been reported for *Saccharomyces cerevisiae*, a yeast, and Gram-negative *E. coli*.[39] Although recovery from ZIF-8-inflicted cell wall damage required 16−20 h before *B. breve* was able to start growing again under unchallenged conditions (see Figure 2C), cell wall damage combined with an acid or antibiotic attack resulted in a severe loss of viability after ZIF-8 encapsulation. Thus, the long recovery period of *B. breve* after ZIF-8 encapsulation combined with the ability of tetracycline to adsorb to ZIF-8 causing high local tetracycline concentration[40] will contribute to the inability of ZIF-8-mineralized shells to kill *E. coli* adhering to intestinal epithelial cell layers under antibiotic exposure.[40]

The *in vitro* demonstrated synergy between alginate-hydrogel-encapsulated *B. breve* and tetracycline in killing tetracycline-resistant adhering *E. coli* is similar to the synergy observed for alginate-hydrogel-encapsulated Lactobacilli working in concert with tobramycin in killing planktonic, multidrug-resistant pathogenic *S. aureus* and *Pseudomonas aeruginosa*.[14] Our study extends the above study by using a different probiotic strain and using bacteria in an adhering rather than in a planktonic state, which is of great relevance for potential clinical applications as most infections are due to adhering pathogens and not the planktonic ones. Bifidobacteria are known to produce biosurfactants[26] and acetate[41] that facilitate detachment of adhering *E. coli* and perturbation of the intracellular anionic composition,[42] respectively. These two processes likely enhance tetracycline entry into *E. coli* to disturb protein synthesis,[43] yielding synergistic *E. coli* killing.

We pre-exposed the probiotic bacteria to simulated gastric acid and therewith mimic the clinical threats encountered by orally administered probiotics combined with antibiotic treatment, including effects on intestinal epithelial layers. Considering the close resemblance between *in vitro* conditions and clinical conditions that can be realized in a transwell co-culture system, it can be debated whether evaluation of probiotic bacteria and their encapsulation require animal experiments. Animal experiments are under heavy societal and regulatory scrutiny while the conditions in an animal experiment are often remote from human clinical conditions,[44] particularly with respect to the different microbiomes in the body. *B. breve*, tetracycline, and calcium alginate are all already used either in the clinic or in over-the-counter products. *B. breve* is orally administered to newborns delivered through cesarean section to ensure a healthy gut microflora.[45] Tetracycline is a frequently used antibiotic in the clinic. Alginate hydrogels are considered safe by the FDA for oral administration.[46] Transplantation of alginate-hydrogel-encapsulated islets of Langerhans successfully increases the control of the blood glucose diabetic type I patients, without invoking an immune response.[47] Accordingly, the *in vitro* demonstrated synergy between alginate-hydrogel-encapsulated *B. breve* and an antibiotic may be clinically pursued, preferably on the basis of enrichment principles[48] to yield a regulatory-approved strategy for the control of antibiotic-resistant *E. coli* infections in the gastrointestinal tract.

CONCLUSIONS

In conclusion, the ZIF-8 shells strongly interacting with *B. breve* cell surfaces caused demonstrable cell wall damage with a minor loss of viability. Accordingly, it took *B. breve* considerably more time to recover from the cell wall damage inflicted by ZIF-8 encapsulation and start growing again than after encapsulation by weakly interacting yolk−shells or alginate hydrogels. Only, alginate hydrogel shells protected *B. breve* against gastric acids and antibiotics and worked synergistically with tetracycline in protecting intestinal epithelial layers against adhering tetracycline-resistant *E. coli* in a transwell co-culture model. This synergy between alginate-hydrogel-encapsulated *B. breve* and an antibiotic warrants further studies for treating antibiotic-resistant *E. coli* infections in the gastrointestinal tract.

ASSOCIATED CONTENT

Supporting Information

The Supporting Information is available free of charge at https://pubs.acs.org/doi/10.1021/acsami.0c21790.

E. coli exposure to tetracycline for different periods of time; narrow scan O_{1s} photoelectron binding energy spectra of unencapsulated and differently encapsulated *B. breve*; zeta potentials and FTIR spectra of *B. breve* prior to and after protamine adsorption and internalization; survival of *B. breve* encapsulated in alginate hydrogel shells using alginate droplets with different volumes for encapsulation during exposure to SGF at pH 2; survival of *E. coli* after culturing with different shell components; and effects of unencapsulated and encapsulated *B. breve* adhering to intestinal epithelial layers on TEER and membrane surface coverage of the epithelial layers grown on transwell membranes (PDF)

AUTHOR INFORMATION

Corresponding Authors

Henny C. van der Mei − *Department of Biomedical Engineering, University of Groningen and University Medical Center Groningen, 9713 AV Groningen, The Netherlands;* orcid.org/0000-0003-0760-8900; Phone: +31 50 361 6094; Email: h.c.van.der.mei@umcg.nl

Henk J. Busscher − *Department of Biomedical Engineering, University of Groningen and University Medical Center Groningen, 9713 AV Groningen, The Netherlands;* Email: h.j.busscher@umcg.nl

Authors

Lu Yuan − *Department of Biomedical Engineering, University of Groningen and University Medical Center Groningen, 9713 AV Groningen, The Netherlands*

Hao Wei − *Department of Biomedical Engineering, University of Groningen and University Medical Center Groningen, 9713 AV Groningen, The Netherlands*

Xiao-Yu Yang − *State Key Laboratory of Advanced Technology for Materials Synthesis and Processing, Wuhan University of Technology, Wuhan 430070, China; School of Engineering and Applied Sciences, Harvard University, Cambridge, Massachusetts 02138, United States*

Wei Geng − *Southern Marine Science and Engineering Guangdong Laboratory (Zhuhai) & School of Chemical Engineering and Technology & School of Materials, Sun Yat-Sen University, Guangdong 510275, China*

https://doi.org/10.1021/acsami.0c21790
ACS Appl. Mater. Interfaces 2021, 13, 15973−15982

Brandon W. Peterson − *Department of Biomedical Engineering, University of Groningen and University Medical Center Groningen, 9713 AV Groningen, The Netherlands;* orcid.org/0000-0002-8969-3696

Complete contact information is available at: https://pubs.acs.org/10.1021/acsami.0c21790

Author Contributions

L.Y. and H.W. contributed equally to this article. The experimental design was made by all authors. The manuscript was written through contributions of all authors. L.Y. and H.W. contributed equally to this work. All authors have approved the final version of the manuscript.

Notes

The authors declare the following competing financial interest(s): HJB is also director of a consulting company SASA BV. The authors declare no potential conflicts of interest with respect to authorship and/or publication of this article. Opinions and assertions contained herein are those of the authors and are not construed as necessarily representing views of the funding organization or their respective employer(s).

■ ACKNOWLEDGMENTS

This work was funded by the University Medical Center Groningen, Groningen, The Netherlands, the Fundamental Research Funds for Central Universities (19lgzd16 and 19lgpy112), the National Science Foundation China (52002414), and the Guangdong Basic and Applied Basic Research Foundation (2019A1515110590).

■ REFERENCES

(1) Praepanitchai, O.-A.; Noomhorm, A.; Anal, A. K. Survival and Behavior of Encapsulated Probiotics (Lactobacillus plantarum) in Calcium-Alginate-Soy Protein Isolate-Based Hydrogel Beads in Different Processing Conditions (pH and Temperature) and in Pasteurized Mango Juice. *BioMed Res. Int.* **2019**, *2019*, 9768152.

(2) Hempel, S.; Newberry, S. J.; Maher, A. R.; Wang, Z.; Miles, J. N. V.; Shanman, R.; Johnsen, B.; Shekelle, P. G. Probiotics for the prevention and treatment of antibiotic-associated diarrhea: a systematic review and meta-analysis. *JAMA* **2012**, *307*, 1959−1969.

(3) Goldenberg, J. Z.; Mertz, D.; Johnston, B. C. Probiotics to Prevent Clostridium difficile Infection in Patients Receiving Antibiotics. *JAMA* **2018**, *320*, 499−500.

(4) Pattani, R.; Palda, V. A.; Hwang, S. W.; Shah, P. S. Probiotics for the Prevention of Antibiotic-Associated Diarrhea and Clostridium difficile Infection among Hospitalized Patients: Systematic Review and Meta-Analysis. *Open Med.* **2013**, *7*, e56−e67.

(5) Champagne, C. P.; Ross, R. P.; Saarela, M.; Hansen, K. F.; Charalampopoulos, D. Recommendations for the Viability Assessment of Probiotics as Concentrated Cultures and in Food Matrices. *Int. J. Food Microbiol.* **2011**, *149*, 185−193.

(6) Vangay, P.; Ward, T.; Gerber, J. S.; Knights, D. Antibiotics, Pediatric Dysbiosis, and Disease. *Cell Host Microbe* **2015**, *17*, 553−564.

(7) Hill, C.; Guarner, F.; Reid, G.; Gibson, G. R.; Merenstein, D. J.; Pot, B.; Morelli, L.; Canani, R. B.; Flint, H. J.; Salminen, S.; Calder, P. C.; Sanders, M. E. Expert Consensus Document: The International Scientific Association for Probiotics and Prebiotics Consensus Statement on the Scope and Appropriate Use of the Term Probiotic. *Nat. Rev. Gastroenterol. Hepatol.* **2014**, *11*, 506−514.

(8) Dodoo, C. C.; Wang, J.; Basit, A. W.; Stapleton, P.; Gaisford, S. Targeted Delivery of Probiotics to Enhance Gastrointestinal Stability and Intestinal Colonisation. *Int. J. Pharm.* **2017**, *530*, 224−229.

(9) Anal, A. K.; Singh, H. Recent Advances in Microencapsulation of Probiotics for Industrial Applications and Targeted Delivery. *Trends Food Sci. Technol.* **2007**, *18*, 240−251.

(10) Reid, G.; Younes, J. A.; Van der Mei, H. C.; Gloor, G. B.; Knight, R.; Busscher, H. J. Microbiota Restoration: Natural and Supplemented Recovery of Human Microbial Communities. *Nat. Rev. Microbiol.* **2011**, *9*, 27−38.

(11) Picot, A.; Lacroix, C. Encapsulation of Bifidobacteria in Whey Protein-Based Microcapsules and Survival in Simulated Gastrointestinal Conditions and in Yoghurt. *Int. Dairy J.* **2004**, *14*, 505−515.

(12) De Castro-Cislaghi, F. P.; Silva, C. D. R. E.; Fritzen-Freire, C. B.; Lorenz, J. G.; Sant'Anna, E. S. *Bifidobacterium* Bb-12 Microencapsulated by Spray Drying with Whey: Survival under Simulated Gastrointestinal Conditions, Tolerance to NaCl, and Viability during Storage. *J. Food Eng.* **2012**, *113*, 186−193.

(13) Li, Y.; Feng, C.; Li, J.; Mu, Y.; Liu, Y.; Kong, M.; Cheng, X.; Chen, X. Construction of Multilayer Alginate Hydrogel Beads for Oral Delivery of Probiotics Cells. *Int. J. Biol. Macromol.* **2017**, *105*, 924−930.

(14) Li, Z.; Behrens, A. M.; Ginat, N.; Tzeng, S. Y.; Lu, X.; Sivan, S.; Langer, R.; Jaklenec, A. Biofilm-Inspired Encapsulation of Probiotics for the Treatment of Complex Infections. *Adv. Mater.* **2018**, *30*, 1803925.

(15) Ianiro, G.; Tilg, H.; Gasbarrini, A. Antibiotics as Deep Modulators of Gut Microbiota: Between Good and Evil. *Gut* **2016**, *65*, 1906−1915.

(16) Levy, J. The Effects of Antibiotic Use on Gastrointestinal Function. *Am. J. Gastroenterol.* **2000**, *95*, S8−S10.

(17) Wang, L.; Li, Y.; Yang, X.-Y.; Zhang, B.-B.; Ninane, N.; Busscher, H. J.; Hu, Z.-Y.; Delneuville, C.; Jiang, N.; Xie, H.; Van Tendeloo, G.; Hasan, T.; Su, B.-L. Single-Cell Yolk-Shell Nanoencapsulation for Long-Term Viability with Size-Dependent Permeability and Molecular Recognition. *Natl. Sci. Rev.* **2020**, nwaa097.

(18) Heidebach, T.; Först, P.; Kulozik, U. Microencapsulation of Probiotic Cells for Food Applications. *Crit. Rev. Food Sci. Nutr.* **2012**, *52*, 291−311.

(19) De Vos, P.; Bučko, M.; Gemeiner, P.; Navrátil, M.; Švitel, J.; Faas, M.; Strand, B. L.; Skjak-Braek, G.; Morch, Y. A.; Vikartovská, A.; Lacik, I.; Kollarikova, G.; Orive, G.; Poncelet, D.; Pedraz, J. L.; Ansorge-Schumacher, M. B. Multiscale Requirements for Bioencapsulation in Medicine and Biotechnology. *Biomaterials* **2009**, *30*, 2559−2570.

(20) Hou, L.; Wu, P. Exploring the Hydrogen-Bond Structures in Sodium Alginate through Two-Dimensional Correlation Infrared Spectroscopy. *Carbohydr. Polym.* **2019**, *205*, 420−426.

(21) Scheiner, S.; Kar, T.; Gu, Y. Strength of the CαH··O Hydrogen Bond of Amino Acid Residues. *J. Biol. Chem.* **2001**, *276*, 9832−9837.

(22) Liang, K.; Richardson, J. J.; Cui, J.; Caruso, F.; Doonan, C. J.; Falcaro, P. Metal-Organic Framework Coatings as Cytoprotective Exoskeletons for Living Cells. *Adv. Mater.* **2016**, *28*, 7910−7914.

(23) Laitaoja, M.; Valjakka, J.; Jänis, J. Zinc Coordination Spheres in Protein Structures. *Inorg. Chem.* **2013**, *52*, 10983−10991.

(24) Rulíšek, L.; Havlas, Z. Theoretical Studies of Metal Ion Selectivity. 1. DFT Calculations of Interaction Energies of Amino Acid Side Chains with Selected Transition Metal Ions (Co2+, Ni2+, Cu2+, Zn2+, Cd2+, and Hg2+). *J. Am. Chem. Soc.* **2000**, *122*, 10428−10439.

(25) John-Henry, K. C.; Donato, K. A.; Shen-Tu, G.; Gordanpour, M.; Sherman, P. M. Lactobacillus rhamnosus strain GG prevents enterohemorrhagic Escherichia coli O157:H7-induced changes in epithelial barrier function. *Infect. Immun.* **2008**, *76*, 1340−1348.

(26) Yuan, L.; van der Mei, H. C.; Busscher, H. J.; Peterson, B. W. Two-Stage Interpretation of Changes in TEER of Intestinal Epithelial Layers Protected by Adhering Bifidobacteria during E. coli Challenges. *Front. Microbiol.* **2020**, *11*, 599555.

(27) Xu, M.; Gagné-Bourque, F.; Dumont, M.-J.; Jabaji, S. Encapsulation of *Lactobacillus casei* ATCC 393 Cells and Evaluation of Their Survival after Freeze-Drying, Storage and under Gastrointestinal Conditions. *J. Food Eng.* **2016**, *168*, 52−59.

(28) Goyal, R. K.; Guo, Y.; Mashimo, H. Advances in the Physiology of Gastric Emptying. *Neurogastroenterol. Motil.* **2019**, *31*, No. e13546.
(29) Schindelin, J.; Arganda-Carreras, I.; Frise, E.; Kaynig, V.; Longair, M.; Pietzsch, T.; Preibisch, S.; Rueden, C.; Saalfeld, S.; Schmid, B.; Tinevez, J.-Y.; White, D. J.; Hartenstein, V.; Eliceiri, K.; Tomancak, P.; Cardona, A. Fiji: An Open-Source Platform for Biological-Image Analysis. *Nat. Methods* **2012**, *9*, 676−682.
(30) Van der Mei, H. C.; De Vries, J.; Busscher, H. J. X-Ray Photoelectron Spectroscopy for the Study of Microbial Cell Surfaces. *Surf. Sci. Rep.* **2000**, *39*, 1−24.
(31) Amory, D. E.; Genet, M. J.; Rouxhet, P. G. Application of XPS to the Surface Analysis of Yeast Cells. *Surf. Interface Anal.* **1988**, *11*, 478−486.
(32) Hall, N. G.; Schönfeldt, H. C. Total Nitrogen vs. Amino-Acid Profile as Indicator of Protein Content of Beef. *Food Chem.* **2013**, *140*, 608−612.
(33) Boonaert, C. J. P.; Rouxhet, P. G. Surface of Lactic Acid Bacteria: Relationships between Chemical Composition and Physicochemical Properties. *Appl. Environ. Microbiol.* **2000**, *66*, 2548−2554.
(34) Szklarczyk, M.; Macak, K.; Roberts, A. J.; Takahashi, K.; Hutton, S.; Głaszczka, R.; Blomfield, C. Sub-Nanometer Resolution XPS Depth Profiling: Sensing of Atoms. *Appl. Surf. Sci.* **2017**, *411*, 386−393.
(35) Ahirrao, S. P.; Gide, P. S.; Shrivastav, B.; Sharma, P. Ionotropic Gelation: A Promising Cross Linking Technique for Hydrogels. *Res. Rev.: J. Pharm. Nanotechnol.* **2014**, *2*, 1−6.
(36) Cuddy, M. F.; Poda, A. R.; Brantley, L. N. Determination of Isoelectric Points and the Role of pH for Common Quartz Crystal Microbalance Sensors. *ACS Appl. Mater. Interfaces* **2013**, *5*, 3514−3518.
(37) Chen, B.; Yang, Z.; Zhu, Y.; Xia, Y. Zeolitic Imidazolate Framework Materials: Recent Progress in Synthesis and Applications. *J. Mater. Chem. A* **2014**, *2*, 16811−16831.
(38) Anselmo, A. C.; McHugh, K. J.; Webster, J.; Langer, R.; Jaklenec, A. Layer-by-Layer Encapsulation of Probiotics for Delivery to the Microbiome. *Adv. Mater.* **2016**, *28*, 9486−9490.
(39) Chen, W.; Kong, S.; Lu, M.; Chen, F.; Cai, W.; Du, L.; Wang, J.; Wu, C. Comparison of Different Zinc Precursors for the Construction of Zeolitic Imidazolate Framework-8 Artificial Shells on Living Cells. *Soft Matter* **2019**, *16*, 270−275.
(40) Li, N.; Zhou, L.; Jin, X.; Owens, G.; Chen, Z. Simultaneous Removal of Tetracycline and Oxytetracycline Antibiotics from Wastewater Using a ZIF-8 Metal Organic-Framework. *J. Hazard. Mater.* **2019**, *366*, 563−572.
(41) Fukuda, S.; Toh, H.; Hase, K.; Oshima, K.; Nakanishi, Y.; Yoshimura, K.; Tobe, T.; Clarke, J. M.; Topping, D. L.; Suzuki, T.; Taylor, T. D.; Itoh, K.; Kikuchi, J.; Morita, H.; Hattori, M.; Ohno, H. Bifidobacteria Can Protect from Enteropathogenic Infection through Production of Acetate. *Nature* **2011**, *469*, 543−547.
(42) Pinhal, S.; Ropers, D.; Geiselmann, J.; De Jong, H. Acetate Metabolism and the Inhibition of Bacterial Growth by Acetate. *J. Bacteriol.* **2019**, *201*, No. e00147-19.
(43) Rasmussen, B.; Noller, H. F.; Daubresse, G.; Oliva, B.; Misulovin, Z.; Rothstein, D. M.; Ellestad, G. A.; Gluzman, Y.; Tally, F. P.; Chopra, I. Molecular Basis of Tetracycline Action: Identification of Analogs Whose Primary Target Is Not the Bacterial Ribosome. *Antimicrob. Agents Chemother.* **1991**, *35*, 2306−2311.
(44) Moriarty, T.; Grainger, D.; Richards, R. Challenges in Linking Preclinical Anti-Microbial Research Strategies with Clinical Outcomes for Device-Associated Infections. *Eur. Cells Mater.* **2014**, *28*, 112−128.
(45) Hurkala, J.; Lauterbach, R.; Radziszewska, R.; Strus, M.; Heczko, P. Effect of a Short-Time Probiotic Supplementation on the Abundance of the Main Constituents of the Gut Microbiota of Term Newborns Delivered by Cesarean Section-A Randomized, Prospective, Controlled Clinical Trial. *Nutrients* **2020**, *12*, 3128.
(46) U.S. Food and Drug Administration. *Food for human consumption: Direct food substances affirmed as generally recognized as safe*, **2020**.
(47) Basta, G.; Montanucci, P.; Luca, G.; Boselli, C.; Noya, G.; Barbaro, B.; Qi, M.; Kinzer, K. P.; Oberholzer, J.; Calafiore, R. Long-Term Metabolic and Immunological Follow-Up of Nonimmunosuppressed Patients With Type 1 Diabetes Treated With Microencapsulated Islet Allografts: Table 1. *Diabetes Care* **2011**, *34*, 2406−2409.
(48) Busscher, H. J.; Alt, V.; Van der Mei, H. C.; Fagette, P. H.; Zimmerli, W.; Moriarty, T. F.; Parvizi, J.; Schmidmaier, G.; Raschke, M. J.; Gehrke, T.; Bayston, R.; Baddour, L. M.; Winterton, L. C.; Darouiche, R. O.; Grainger, D. W. A Trans-Atlantic Perspective on Stagnation in Clinical Translation of Antimicrobial Strategies for the Control of Biomaterial-Implant-Associated Infection. *ACS Biomater. Sci. Eng.* **2019**, *5*, 402−406.

https://doi.org/10.1021/acsami.0c21790
ACS Appl. Mater. Interfaces 2021, 13, 15973−15982